JACS
JOURNAL OF THE AMERICAN CHEMICAL SOCIETY

Article

pubs.acs.org/JACS

Systematic Investigation of Benzodithiophene- and Diketopyrrolopyrrole-Based Low-Bandgap Polymers Designed for Single Junction and Tandem Polymer Solar Cells

Letian Dou,[†] Jing Gao,[†] Eric Richard,[†] Jingbi You,[†] Chun-Chao Chen,[†] Kitty C. Cha,[†] Youjun He,[†] Gang Li,[†] and Yang Yang*[,†,‡]

[†]Department of Materials Science and Engineering, and [‡]California NanoSystems Institute, University of California, Los Angeles, California 90095, United States

Supporting Information

ABSTRACT: The tandem solar cell architecture is an effective way to harvest a broader part of the solar spectrum and make better use of the photonic energy than the single junction cell. Here, we present the design, synthesis, and characterization of a series of new low bandgap polymers specifically for tandem polymer solar cells. These polymers have a backbone based on the benzodithiophene (BDT) and diketopyrrolopyrrole (DPP) units. Alkylthienyl and alkylphenyl moieties were incorporated onto the BDT unit to form BDTT and BDTP units, respectively; a furan moiety was incorporated onto the DPP unit in place of thiophene to form the FDPP unit. Low bandgap polymers (bandgap = 1.4−1.5 eV) were prepared using BDTT, BDTP, FDPP, and DPP units via Stille-coupling polymerization. These structural modifications lead to polymers with different optical, electrochemical, and electronic properties. Single junction solar cells were fabricated, and the polymer:$PC_{71}BM$ active layer morphology was optimized by adding 1,8-diiodooctane (DIO) as an additive. In the single-layer photovoltaic device, they showed power conversion efficiencies (PCEs) of 3−6%. When the polymers were applied in tandem solar cells, PCEs over 8% were reached, demonstrating their great potential for high efficiency tandem polymer solar cells.

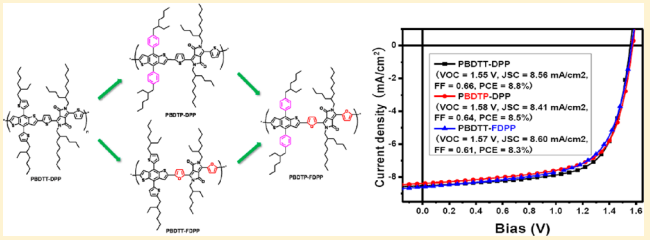

1. INTRODUCTION

Organic photovoltaics (OPV) technology has great potential for low-cost solar electrical energy generation and has drawn a great deal of attention.[1−4] Tremendous efforts on processing, material, and device have been devoted to this field in recent years to improve the efficiency, with record efficiencies being reported both in polymer solar cells (PSCs) and in small-molecule OPV, both in the academia field and industry (PSCs) and small-molecule OPV both in the academia field and in industry (e.g., Solarmer Energy Inc., Kornaka Inc., Mitsubishi Chemical, and Heliatek).[5−9] Polymer-based OPV attracts more attention due to its easy synthesis and purification as well as better processability. So far in the literature, single junction PSCs based on conjugated polymers as electron-donor materials blended with [6,6]-phenyl-C_{71}-butyric acid methyl ester ($PC_{71}BM$) as an electron-acceptor material have achieved around 8% power conversion efficiency (PCE) using a bulk heterojunction (BHJ) device structure.[10−12] However, further increasing PCE is challenging for single junction devices, because photons with energy smaller than the bandgap cannot be absorbed (loss of photocurrent) and photons with larger energy will lose their excess energy via a thermalization process of the hot carriers (loss of photovoltage).[13] Alternatively, tandem solar cells can reduce these losses by using separate subcells, each converting a different part of the solar spectrum.[14−17] For example, the Shockley−Quiesser limitation of single junction solar cell is ∼34% (this requires a semiconducting material with E_g ∼1.4 eV).[18] Via enhancing photon utilization efficiency, inorganic multijunction tandem solar cells have reached up to 43.5% efficiency.[8,9] Using conservative assumptions, Brabec et al. predicted that the theoretical maximum PCE for a tandem polymer solar cell is 15%, whereas it is 10% for a single junction cell.[19,20] Realizing solution processed tandem solar cell is very promising for achieving high efficiency and low cost photovoltaic devices.

Most of the work on tandem PSCs has focused on the double junction structure, which consists of a front cell with a high-bandgap material, an interconnecting layer (ICL), and a rear cell with a low-bandgap (LBG) material.[21−24] Most of those studies have focused on improving the ICL, and only a few have demonstrated high efficiencies of 4−7%.[25−30] In addition to the ICL, the photoactive materials also play a critical role in determining the PCE. One of the problems holding back the progress of tandem solar cell is the lack of a high performance low bandgap polymer (E_g < 1.5 eV), designed for the tandem structure. As a result, the efficiency for previous tandem solar cells has been limited to below 7%

Received: February 13, 2012

   dx.doi.org/10.1021/ja301460s | J. Am. Chem. Soc. XXXX, XXX, XXX−XXX

for awhile.[21−30] Poly[2,6-(4,4-bis-(2-ethylhexyl)-4*H*-cyclopenta[2,1-*b*;3,4-*b*′]dithiophene)-*alt*-4,7-(2,1,3-benzothiadiazole)] (PCPDTBT) was the first polymer demonstrated to be highly effective in tandem PSCs, and a PCE of 6.5% was reported by Heeger et al. in 2007.[6,25] Later, our group replaced a carbon atom of PCPDTBT with a silicon atom and achieved a LBG polymer poly[(4,4′-bis(2-ethylhexyl)dithieno[3,2-*b*:2′,3′-*d*]silole)-2,6-diyl-*alt*-(2,1,3-benzothiadiazole)-4,7-diyl] (PSBTBT).[31] Tandem devices based on this material, together with a newly developed robust ICL, showed 7% PCE.[26] Another important tandem PSC with 4.9% PCE was reported by Janssen et al. with the LBG polymer poly[3,6-bis(4′-dodecyl-[2,2′]bithiophenyl-5-yl)-2,5-bis(2-ethylhexyl)-2,5-dihydropyrrolo[3,4-]pyrrole-1,4-dione] (pBBTDPP2).[23]

It is worth mentioning that the diketopyrrolopyrrole (DPP) unit, which was developed over four decades ago for high-performance pigments, appeared to be a promising building block for LBG polymers.[32] It is highly absorbing in the visible region and strongly electron withdrawing. When polymerized with electron-donating monomers, the resulting polymers show energy bandgaps smaller than 1.5 eV. In recent years, there has been an intensive effort to develop LBG polymers based on the DPP unit for photovoltaic applications, and single junction devices with PCEs of 4−5% were reported by Janssen, Fréchet, and Yang.[33−36] Because of poor solubility, relatively low molecular weights, and high highest occupied molecular orbital (HOMO) levels, the devices showed either low open circuit voltage (V_{OC}), low short circuit current (J_{SC}), or low fill factor (FF). They are far from ideal for a tandem structure because when two subcells are connected in series, the overall tandem cell performance will be limited by the poorest-performing subcell.

Recently, we have demonstrated a tandem PSC with National Renewable Energy Laboratory (NREL) certified efficiency of 8.62%, incorporating a new LBG polymer, PBDTT-DPP, based on alternating DPP and alkylthienylbenzodithiophene (BDTT) units (Figure 1).[37] However, the

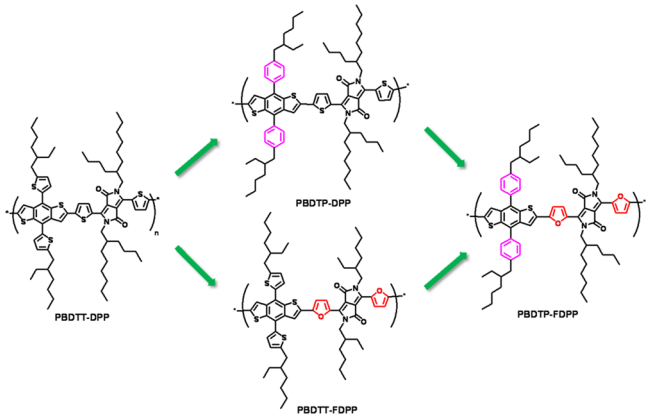

Figure 1. Chemical structures of PBDTT-DPP, PBDTP-DPP, PBDTT-FDPP, and PBDTP-FDPP.

detailed synthesis and characterization of this new family of LBG polymers have not been reported. Here, we report the design, synthesis, and characterization of a series of polymers for tandem PSCs derived from modification of PBDTT-DPP (Scheme 1). To tune the structural and electronic properties, a new monomer (BDTP) with an alkylphenyl group attached to the BDT unit instead of the alkylthienyl group was developed; a

Scheme 1. Synthesis of Monomers, PBDTT-DPP, PBDTP-DPP, PBDTT-FDPP, and PBDTP-FDPP[a]

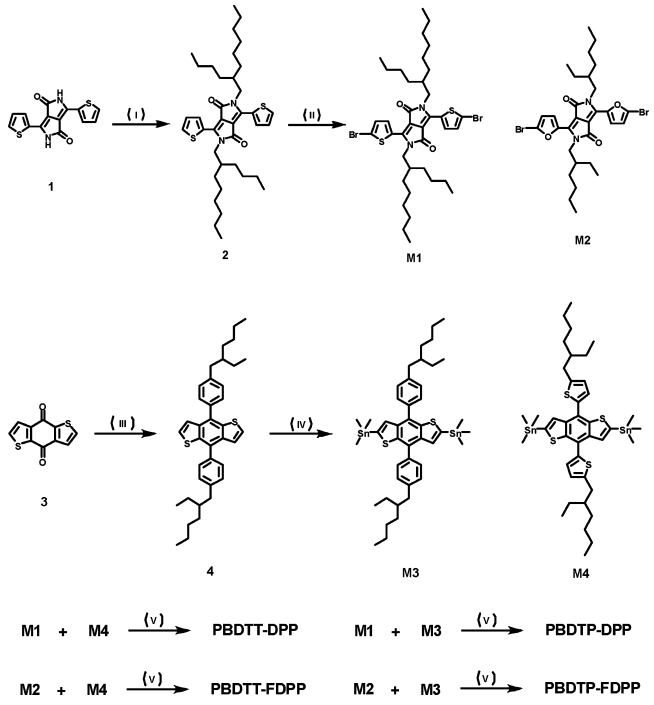

[a](I) 2-Butyloctyl bromide, K_2CO_3, DMF, 140 °C. (II) NBS, $CHCl_3$, room temperature. (III) 4-(2-Ethylhexyl)bromobenzene, Mg, then $SnCl_2{\cdot}2H_2O$, THF, room temperature. (IV) *n*-Butyl lithium, then $SnMe_3Cl$, in THF, room temperature. (V) $Pd(PPh_3)_4$, toluene/DMF, 110 °C.

furan group was incorporated into the DPP unit to form the FDPP unit using a reported method.[35] Both BDTT (**M4**) and BDTP (**M3**) were polymerized with DPP (**M1**) and FDPP (**M2**) via Stille-coupling polymerization. Four polymers, PBDTT-DPP, PBDTP-DPP, PBDTT-FDPP, and PBDTP-FDPP, were obtained in good yield. As compared to early efforts on DPP based polymers, the newly designed polymers show deeper HOMO levels and better charge transport properties, which lead to higher V_{OC} and J_{SC} in PSC devices. The low energy bandgap (1.4−1.5 eV) and high photovoltaic performance enable them to be applied in tandem PSCs, and PCEs close to 9% were achieved.

2. EXPERIMENTAL SECTION

Materials. Benzo[1,2-*b*:4,5-*b*′]dithiophene-4,8-dione (**3**), 2,5-diethylhexyl-3,6-bis(5-bromofuran-2-yl)pyrrolo[3,4-*c*]-pyrrole-1,4-dione (**M2**), 2,6-bis(trimethyltin)-4,8-bis(5-ethylhexyl-2-thienyl)-benzo[1,2-*b*:4,5-*b*′]dithiophene (**M4**), 4-ethylhexylbromobezene, 2-ethylhexylthiophene, and Indene-C_{60} bisadduct (ICBA) were synthesized according to the procedures reported in the literature.[7,35,38] Poly(3-hexylthiophene) (P3HT) was purchased from Rieke Metals. [6,6]-Phenyl-C_{71}-butyric acid methyl ester ($PC_{71}BM$) was purchased from Nano-C. Unless otherwise stated, all of the chemicals were purchased from Aldrich and used as received. The monomers and polymers were synthesized according to Scheme 1.

3,6-Dithiophen-2-yl-2,5-dihydropyrrolo[3,4-*c*]pyrrole-1,4-dione (1). Potassium *tert*-butoxide (20 g, 180 mmol) was added to a round-bottom flask with argon protection. A solution of *t*-amyl alcohol (125 mL) and 2-thiophenecarbonitrile (16.4 g, 150 mmol) was injected in one portion. The mixture was warmed to 100−110 °C, and a solution of dimethyl succinate (7.30 g, 50 mmol) in *t*-amyl alcohol (40 mL) was dropped in slowly in 1 h. The reaction was kept at the

dx.doi.org/10.1021/ja301460s | *J. Am. Chem. Soc.* XXXX, XXX, XXX−XXX

same temperature for about 1 h, and then the methanol byproduct was distilled off and the reaction was kept at 100−110 °C for another 2 h. The mixture was then cooled to 65 °C, diluted with 50 mL of methanol, neutralized with acetic acid, and refluxed for another 10 min. Next the suspension was filtered, and the black filter cake was washed with hot methanol and water twice and dried in a vacuum to get the crude product, which could be used directly in the next step without further purification (10.6 g, yield 72%).

2,5-Dibutyloctyl-3,6-dithiophen-2-ylpyrrolo[3,4-*c*]pyrrole-1,4-dione (2). Compound **1** (13.0 g, 43.3 mmol) and anhydrous potassium carbonate (24 g, 173 mmol) were dissolved into *N*,*N*-dimethylformamide (250 mL) in a two-neck round flask and heated to 145 °C under argon protection. 2-Butyloctyl bromide (49.8 g, 200 mmol) was injected in one portion by syringe. After the reaction was stirred for 12 h at 145 °C, the solution was cooled to room temperature, poured into 500 mL of icewater, and then filtered. The filter cake was washed with water and methanol several times. After being dried in a vacuum, the crude product was purified by silica gel chromatography using dichloromethane as eluent to obtain a purple-black solid powder (17.3 g, yield 76%). ^{1}H NMR ($CDCl_3$, 400 MHz): 8.93 (d, 2H), 7.63 (d, 2H), 7.28 (d, 2H), 4.06 (m, 4H), 1.76 (m, 2H), 1.43−1.25 (m, 32H), 0.87 (m, 12H). MS: 636.2 (calculated: 636.4).

2,5-Dibutyloctyl-3,6-bis(5-bromothiophen-2-yl)pyrrolo[3,4-*c*]-pyrrole-1,4-dione (M1). Compound **2** (5.47 g, 8.62 mmol) and *N*-bromosuccinimide (3.14 g, 17.6 mmol) were dissolved into chloroform (100 mL) in a two-neck round-bottom flask under argon protection, and then the solution was protected from light and stirred at room temperature. After 40 h, the mixture was poured into 400 mL of methanol and then filtered. The filter cake was washed with hot methanol twice. After drying in a vacuum, the pure product was obtained as a purple-black solid (5.21 g, yield 76%). ^{1}H NMR ($CDCl_3$, 400 MHz): d = 8.61 (d, 2H), 7.22 (d, 2H), 3.92 (d, 4H), 1.88 (m, 2H), 1.49−1.21 (br, 32H), 0.85 (t, 12H). ^{13}C NMR ($CDCl_3$, 100 MHz): d = 161.38, 139.38, 135.29, 131.42, 131.16, 118.98, 108.00, 46.31, 37.72, 31.76, 31.15, 30.86, 29.65, 28.38, 26.14, 23.03, 22.64, 14.09, 14.02 ppm. MS: 792.5 (calculated: 792.2).

4,8-Bis(4-ethylhexyl-1-phenyl)-benzo[1,2-*b*:4,5-*b*′]-dithiophene (4). Under protection of argon, 1-bromo-4-(2-ethylhexyl)benzene (4.96 g, 18.4 mmol) was added slowly to magnesium turnings (0.538 g, 22.1 mmol) in anhydrous THF (22 mL) with a catalytic amount of I_2 (∼10 mg). The mixture was maintained at reflux until the color of the solution became dark and the magnesium began to be consumed (1−5 h). Reflux was continued one more hour, and then the solution was cooled to room temperature. The solution was added slowly to 4,8-dehydrobenzo-[1,2-*b*:4,5-*b*′]dithiophene-4,8-dione (1.35 g, 6.15 mmol) suspended in 10 mL of THF at room temperature. The temperature was maintained at 50 °C for 1 h. The diketone dissolved to form a brown solution. $SnCl_2$ (8.9 g) dissolved in 10% aqueous HCl (12.4 mL) was added dropwise, and the mixture was stirred one more hour at 50 °C. The reaction mixture was poured into water (100 mL) and extracted with ether (100 mL), washed three times with water (100 mL), and then 50 mL of saturated $NaHCO_3$. The residue of the organic phase after evaporation was purified by chromatography on silica gel with pure hexane to give the title compound as a yellow-green oil (1.63 g, 47% yield), which crystallized upon standing. ^{1}H NMR ($CDCl_3$, 400 MHz): d = 7.81 (d, 4H), 7.64 (d, 4H), 7.36 (m, 4H), 2.76 (t, 4H), 1.76 (m, 2H), 1.49−1.21 (br, 16H), 0.88 (t, 12H). MS: 567.0 (calculated: 566.3).

2,6-Bis(trimethyltin)-4,8-bis(4-ethylhexyl-1-phenyl)-benzo-[1,2-*b*:4,5-*b*′]dithiophene (M3). Under protection of argon at room temperature, 1.6 M *n*-butyllithium solution in hexanes (4.23 mL, 6.77 mmol) was added dropwise to 4,8-bis-(4-(2-ethylhexyl)phenyl)benzo-[1,2-*b*:4,5-*b*′]dithiophene (1.62 g, 2.82 mmol) dissolved in 30 mL of THF. The solution was warmed to 40 °C for 1 h, and then 1.0 M trimethyltin chloride solution in THF (7.34 mL, 7.34 mmol) was added. The reaction mixture was poured into water (100 mL) and extracted with ether (50 mL). The ether phase was evaporated, and the residue was recrystallized from 20 mL of acetone to afford the title compound in 65% yield (1.54 g). ^{1}H NMR ($CDCl_3$, 400 MHz): d = 7.64 (d, 4H), 7.39 (d, 4H), 7.38 (s, 2H), 2.69 (t, 4H), 1.79 (m, 2H), 1.44−1.30 (br, 16H), 0.90 (t, 12H), 0.35 (t, 18H). ^{13}C NMR ($CDCl_3$, 100 MHz): d = 142.45, 141.63, 137.10, 130.84, 129.52, 129.19, 128.84, 41.08, 40.19, 32.48, 28.94, 25.78, 23.04, 14.16, 10.93, −8.22 ppm. MS: 792.5 (calculated: 792.2).

Polymerization for PBDTP-DPP. M1 (0.1952 g, 0.2456 mmol) and compound **M4** (0.2360 g, 0.2456 mmol) were dissolved into 10 mL of toluene and 1 mL of DMF in a flask protected by argon. The solution was flushed with argon for 10 min, and then 10 mg of $Pd(PPh_3)_4$ was added into the flask. The solution was flushed with argon again for 20 min. The oil bath was heated to 110 °C gradually, and the reaction mixture was stirred for 10 h at 110 °C under argon atmosphere. Next, the mixture was cooled to room temperature, and the polymer was precipitated by addition of 100 mL of methanol and the precipitated solid was collected and purified by Soxhlet extraction. The title polymer was obtained as a dark green-purple solid, yield 30%. The polymer can be readily dissolved into THF, chloroform, chlorobenzene, or dichlorobenzene, etc. The polymer was thermally stable up to 290 °C (3% weight loss by TGA). ^{1}H NMR (400 MHz, $CDCl_3$): d = 6.7−8.6 (br, 10H), 1.8−4.9 (br, 14H), 0.6−1.5 (br, 78H). M_n = 40.7 k; polydispersity = 2.2.

Polymerization for PBDTP-DPP. PBDTP-DPP was prepared using the same procedure as PBDTT-DPP. The polymer was thermally stable up to 300 °C (3% weight loss by TGA). ^{1}H NMR (400 MHz, $CDCl_3$): d = 6.5−8.6 (br, 14H), 1.8−4.5 (br, 14H), 0.6−1.5 (br, 78H). M_n = 36.3 k; polydispersity = 1.9.

Polymerization for PBDTT-FDPP. PBDTT-FDPP was prepared using the same procedure as PBDTT-DPP. The polymer was thermally stable up to 275 °C (3% weight loss by TGA). ^{1}H NMR (400 MHz, $CDCl_3$): d = 6.4−8.6 (br, 10H), 1.8−4.2 (br, 14H), 0.6−1.5 (br, 62H). M_n = 28.8 k; polydispersity = 2.2.

Polymerization for PBDTP-FDPP. PBDTP-FDPP was prepared using the same procedure as PBDTT-DPP. The polymer was thermally stable up to 285 °C (3% weight loss by TGA). ^{1}H NMR (400 MHz, $CDCl_3$): d = 6.7−8.8 (br, 14H), 1.7−4.8 (br, 14H), 0.6−1.6 (br, 62H). M_n = 20.9 k; polydispersity = 2.0.

Characterization. ^{1}H and ^{13}C NMR spectra were measured on a Bruker ARX-400 spectrometer. Absorption spectra were taken on a Varian Cary 50 ultraviolet−visible spectrometer. The molecular weight of the polymers was measured by the GPC method, and polystyrene was used as a standard and chloroform was used as eluent. TGA measurement was performed on a Perkin-Elmer TGA-7. The electrochemical cyclic voltammetry (CV) was conducted with Pt disk, Pt plate, and Ag/AgCl electrode as working electrode, counter electrode, and reference electrode, respectively, in a 0.1 mol/L tetrabutylammonium hexafluorophosphate (Bu_4NPF_6) acetonitrile solution. The polymer films for electrochemical measurements were coated from a polymer chloroform solution, ca. 5 mg/mL. For calibration, the redox potential of ferrocene/ferrocenium (Fc/Fc^+) was measured under the same conditions, and it is located at 0.39 V vs the Ag/AgCl electrode. It is assumed that the redox potential of Fc/Fc^+ has an absolute energy level of −4.80 eV to vacuum. The energy levels of the highest (HOMO) and lowest unoccupied molecular orbital (LUMO) were then calculated according to the following equations:

$$E_{HOMO} = -(\varphi_{ox} + 4.41)(eV),\ E_{LUMO} = -(\varphi_{re} + 4.41)(eV)$$

where φ_{ox} is the onset oxidation potential vs Ag/AgCl and φ_{re} is the onset reduction potential vs Ag/AgCl.

Device Fabrication. Regular Structure Single Cell. PBDTT-DPP, PBDTT-FDPP, or PBDTP-FDPP was codissolved with $PC_{71}BM$ in 1,2-dichlorobenzene (DCB) with a weight ratio of 1:2 with a concentration of 8 mg/mL. PBDTP-DPP was codissolved with $PC_{71}BM$ in chloroform with a weight ratio of 1:2 and a concentration of 5 mg/mL. Mixed solvents with about 1−4% (volume) 1,8-diiodooctance were used to further improve the device performances. ITO-coated glass substrates (15 Ω/cm^2) were cleaned stepwise in detergent, water, acetone, and isopropyl alcohol under ultrasonication for 15 min each and subsequently dried in an oven for 5 h. A thin layer (∼30 nm) of PEDOT:PSS (Baytron P VP A1 4083) was spin-coated onto the ITO surface, which was pretreated by ultraviolet ozone for 15

dx.doi.org/10.1021/ja301460s | J. Am. Chem. Soc. XXXX, XXX, XXX−XXX

min. Low-conductivity PEDOT:PSS was chosen to minimize measurement error from device area due to lateral conductivity of PEDOT:PSS. After being baked at 120 °C for ~20 min, the substrates were transferred into a nitrogen-filled glovebox (<0.1 ppm O_2 and H_2O). A polymer/$PC_{71}BM$ composite layer (ca. 100 nm thick) was then spin-cast from the blend solutions at 2500 rpm on the ITO/PEDOT:PSS substrate without further special treatments. The film was then transferred into a thermal evaporator, which is located in the same glovebox. A Ca layer (20 nm) and an Al layer (100 nm) were deposited in sequence under a vacuum of 2×10^{-6} Torr. The effective area of the device was measured to be 0.10 cm^2.

Inverted Tandem Cells. The device architecture of the tandem solar cell is shown in Figure S5. The precleaned ITO substrates were treated with UV-ozone. The P3HT:ICBA[38] at a 1:1 weight ratio in 1.8% DCB solution was spin-casted at 800 rpm for 30 s on top of a layer of ZnO (the synthesis of ZnO nanoparticles can be found in ref 39). The films were annealed at 150 °C for 10 min. PEDOT:PSS was spin-coated on the first active layer and annealed at 150 °C for 10 min. After that, a thin layer of ZnO film was spin-cast, followed by thermal annealing at 150 °C for 10 min. Polymer:$PC_{71}BM$ (1:2) from 8 mg/mL DCB solution was then spin-coated without any subsequent processing. The device fabrication was completed by thermal evaporation of 15 nm MoO_3 and 100 nm Ag as the anode under vacuum at a base pressure of 2×10^{-6} Torr. The effective area of the device was measured to be 0.10 cm^2.

Hole Mobility. Hole mobility was measured using the space charge limited current model (SCLC),[40] using a diode configuration of ITO/PEDOT:PSS/polymer:$PC_{71}BM$/Au and taking current−voltage measurements in the range of 0−6 V and fitting the results to a space charge limited form, where the SCLC is described by:

$$J = (8/9)\varepsilon_r\varepsilon_0\mu_e(V^2/L^3)$$

where ε_0 is the permittivity of free space, ε_r is the dielectric constant of the polymer, μ is the hole mobility, V is the voltage drop across the device ($V = V_{appl} - V_r - V_{bi}$, where V_{appl} is the applied voltage to the device, V_r is the voltage drop due to contact resistance and series resistance across the electrodes, and V_{bi} is the built-in voltage due to the difference in work function of the two electrodes), and L is the polymer thickness. The dielectric constant ε_r is assumed to be 3, which is a typical value for conjugated polymers. The thickness of the polymer films is measured by using a Dektak profilometer.

Current−Voltage Measurement. The fabricated device was encapsulated in a nitrogen-filled glovebox by UV cured epoxy and a cover glass. The current density−voltage (J−V) curves were measured using a Keithley 2400 source-measurement unit. The photocurrent was measured under AM 1.5 G illumination at 100 mW/cm^2 under a Newport Thermal Oriel 91192 1000W solar simulator. The light intensity was determined by a KG-5 filter diode (traceable to NREL calibration) as a reference cell, followed by the calculation of spectral mismatch factor and then short circuit current (J_{SC}) correction. External quantum efficiencies were measured using a lock-in amplifier (SR830, Stanford Research Systems) with current preamplifier (SR570, Stanford Research Systems) under short-circuit conditions. The devices were illuminated by monochromatic light from a xenon lamp passing through a monochromator (SpectraPro-2150i, Acton Research Corp.) with a typical intensity of 10 μW. The photocurrent signal is then amplified by an SR570 and detected with an SR830. A calibrated monosilicon diode with known spectral response is used as a reference.

AFM Measurement. AFM samples are prepared as follows: Films of polymer/$PC_{71}BM$ blend are cast from solutions with or without 1,8-diiodooctane treatment (ratio following best device conditions), respectively, on clean glass slides. Both pristine and treated films are examined by an Automated Nanite A atomic force microscope. Figure 5 shows the tapping mode phase images of these blend films.

3. RESULTS AND DISCUSSION

Material Design and Synthesis. As we demonstrated, by using three design principles for LBG polymers for tandem cells, (1) lowering the bandgap for spectral matching with the front cell, (2) controlling HOMO/LUMO levels to enhance V_{OC}, and (3) increasing the molecular weight to enhance J_{SC} and FF, high photovoltaic performance can be achieved.[37] The encouraging results of PBDTT-DPP led us to choose its polymer backbone as the structural platform to investigate structure/property relationships of new polymers. Following the three guidelines, a series of LBG polymers were designed and synthesized. The synthesis of BDTT, DPP, and FDPP was performed according to previously reported methods.[35,36,41] The new monomer BDTP was synthesized via a Grignard reaction as shown in Scheme 1. 4-Alkyl bromobenzene was treated with magnesium in tetrahydrofuran (THF) under argon protection to form the Grignard reagent, and then the reagent was transferred to another flask containing benzodithiophenedione dispersed in THF under argon protection. The nucleophilic reaction completed upon heating to 50 °C for several hours. After reduction by $SnCl_2$, 4,8-bis(4-ethylhexyl-1-phenyl)-benzo[1,2-*b*:4,5-*b*′]dithiophene was obtained as a yellow-green oil. It is noteworthy that the butyl-lithium method[41] used for the synthesis of BDTT does not work for BDTP, probably due to the poor stability of the alkylphenyl anion upon heating. We believe that the successful synthetic route of the BDTP unit reported here is of great importance for the OPV community because it provides a promising new family of weak electron-donating units with large π-conjugated systems and good planarity.

It is important to note that the alkyl side chain of the polymers plays a critical role in determining the solar cell performance.[42] In this work, PBDTT-DPP with different alkyl chains was synthesized to find the optimum side chain length. Both *n*-octyl and 2-ethylhexyl chains were used on the BDTT unit, and 2-ethylhexyl, 2-butyloctyl, and 2-hexyldecyl chains were grafted on the DPP unit. Among the six combinations, it is interesting that only the one shown in Figure 1 performs well. Shorter alkyl chains led to very poor solubility (cannot be used for solution processing), and longer alkyl chains led to very good solubility but low J_{SC} in single junction devices (4−6 mA/cm^2). The preliminary photovoltaic performance data of two representative polymers with 2-hexyldecyl chains on DPP unit are shown in the Supporting Information, Figure S1. Thus, the combination of 2-ethylhexyl on BDTT and 2-butyloctyl on DPP was chosen for all other polymers reported here except for FDPP, which showed better performance using shorter alkyl chains as reported.[35] On the basis of the optimized side chain, monomers **M1**, **M2**, **M3**, and **M4** were synthesized as shown in Scheme 1. PBDTT-DPP, PBDTP-DPP, PBDTT-FDPP, and PBDTP-FDPP were synthesized via a Stille-coupling reaction. The structures of polymers were characterized with ^{1}HNMR spectroscopy; all were consistent with the proposed ones. Gel permeation chromatography (GPC) studies showed that these polymers have similar molecular weights (M_n) between 20.9k and 40.7k with a relatively narrow polydispersity index (PDI) around 2 as listed in Table 1. These polymers have good solubility in chlorinated solvents such as chloroform (CF), chlorobenzene (CB), and dichlorobenzene (DCB) except that PBDTP-DPP can only be dissolved in CF beyond 5 mg/mL. Thermogravimetric analysis (TGA) indicates that the polymers are stable up to about 270 °C.

Optical and Electrochemical Properties. The absorption spectra of the polymer films are showed in Figure 2a, and characteristics of the polymers absorption are summarized in Table 1. The polymers have similar optical bandgap around

dx.doi.org/10.1021/ja301460s | J. Am. Chem. Soc. XXXX, XXX, XXX−XXX

Table 1. Molecular Weights and Absorption Properties of the Polymers

polymers	M_n (kDa)	PDI	λ_{peak} (nm)	λ_{onset} (nm)	E_g^{opt} (eV)
PBDTT-DPP	40.7	2.2	710/769	858	1.44
PBDTP-DPP	36.3	1.9	687/753	849	1.46
PBDTT-FDPP	28.8	2.2	681/757	800	1.55
PBDTP-FDPP	20.9	2.0	676/752	816	1.52

1.4−1.5 eV. Because of the weaker electron-donating property of the phenyl group as compared to thienyl group on BDT, PBDTP-DPP and PBDTP-FDPP show slightly higher bandgap than BDTT-based polymers. All of these polymers show absorption ranges from 600 to 800 nm. Among them, PBDTP-DPP and PBDTP-FDPP showed stronger absorption from 600 to 700 nm. Because they all showed very similar absorption in solution (see the Supporting Information, Figure S2), the broader absorption of PBDTP-DPP and PBDTP-FDPP in the solid state was possibly caused by stronger interchain aggregation. As compared to the absorption spectrum of poly(3-hexylthiophene) (P3HT, E_g ~1.9 eV, Figure 2a), which is the most commonly used front-cell material, the overlap of the spectra of the LBG polymers and P3HT is small, and these materials cover the solar spectrum from 350 to 850 nm complementarily, indicating a good match for the tandem structure. The HOMO and LUMO energy levels of the polymers were determined by cyclic voltammetry (CV), and the results are summarized in Figure 2b (the original data can be found in the Supporting Information, Figure S3). Because of the higher ionization potential of benzene and furan, the electron densities are expected to be lower for these moieties than thiophene.[33] Thus, by replacing the thiophene moiety with benzene or furan moieties, the HOMO values of the resulting polymers are expected to be lower, which will lead to higher V_{OC} in photovoltaic devices. The CV results reveal that both PBDTP-DPP and PBDTP-FDPP have lower HOMO levels and larger electrochemical bandgaps than PBDTT-DPP, but PBDTT-FDPP has a slightly higher HOMO level and smaller electrochemical bandgap.

Hole Mobility. Hole mobility of the polymer:$PC_{71}BM$ blends was measured using the space charge limited current (SCLC) model, and the $J-V$ characteristics are plotted in Figure S4 (see the Supporting Information). The hole mobilities of $3.1 \pm 1.0 \times 10^{-4}$, $2.2 \pm 1.0 \times 10^{-4}$, $8.8 \pm 1.0 \times 10^{-4}$, and $4.5 \pm 1.0 \times 10^{-4}$ $cm^2/V{\cdot}s$ were found for PBDTT-DPP, PBDTP-DPP, PBDTT-FDPP, and PBDTP-FDPP, respectively. It is interesting to note that polymers containing the FDPP unit showed higher hole mobility ($8.8 \pm 1.0 \times 10^{-4}$ and $4.5 \pm 1.0 \times 10^{-4}$ $cm^2/V{\cdot}s$) than polymers with the DPP unit ($3.1 \pm 1.0 \times 10^{-4}$ and $2.2 \pm 1.0 \times 10^{-4}$ $cm^2/V{\cdot}s$). This may be attributed to weaker steric hindrance of the shorter side chain on the FDPP unit (2-ethylhexyl) than that on the DPP unit (2-butyloctyl), which led to better $\pi-\pi$ interaction between polymer backbones. Also, it was found that polymers containing the BDTT unit showed higher hole mobility than polymers with BDTP unit ($(8.8 \pm 1.0) \times 10^{-4}$ vs $(4.5 \pm 1.0) \times 10^{-4}$ $cm^2/V{\cdot}s$ for FDPP-based polymers and $(3.1 \pm 1.0) \times 10^{-4}$ vs $(2.2 \pm 1.0) \times 10^{-4}$ $cm^2/V{\cdot}s$ for DPP-based polymers), indicating the thienyl-based BDTT unit is possibly a better hole transporting moiety than the phenyl-based BDTP unit.

Regular Single Layer BHJ Solar Cell Performance. Photovoltaic properties of the polymers were investigated first in single junction solar cells with the regular structure of ITO/PEDOT:PSS/polymer:$PC_{71}BM$/Ca/Al. The polymer active layers were spin-coated from a DCB solution except for PBDTP-DPP, which was coated from CF. The ratio of polymer to $PC_{71}BM$ was adjusted from 1:1 to 1:3 (by weight), and the optimized condition was 1:2 for all of them. To make sure the optimized morphology was being achieved for the blends, we studied the effect of adding 1,8-diiodooctane (DIO) as an additive in detail.[6] Solutions with DIO concentrations varying from 0% to 4% (by volume) were prepared and used to coat the active layer. In most of the high performance LBG polymer systems reported so far, adding a certain amount of DIO can facilitate the formation of nanoscale phase separation of polymer:PCBM blends during spin-coating and thus enhance the PCE greatly. For example, PCPDTBT[6] showed 5.5% PCE versus 2.8% upon adding 2% DIO, PTB4[7] showed 6.1% PCE versus 3.1% upon adding 3% DIO, and PDPPTPT[34] showed 5.5% PCE versus 2.0% upon adding 3% DIO. Interestingly, we found that the four polymers in this work, which are similar in structure, showed very different responses to the addition of DIO in the solution, and one of them gave the best performance without adding any DIO.

Figure 3 shows the V_{OC}, J_{SC}, FF, and PCE results as a function of DIO concentration for the single junction devices

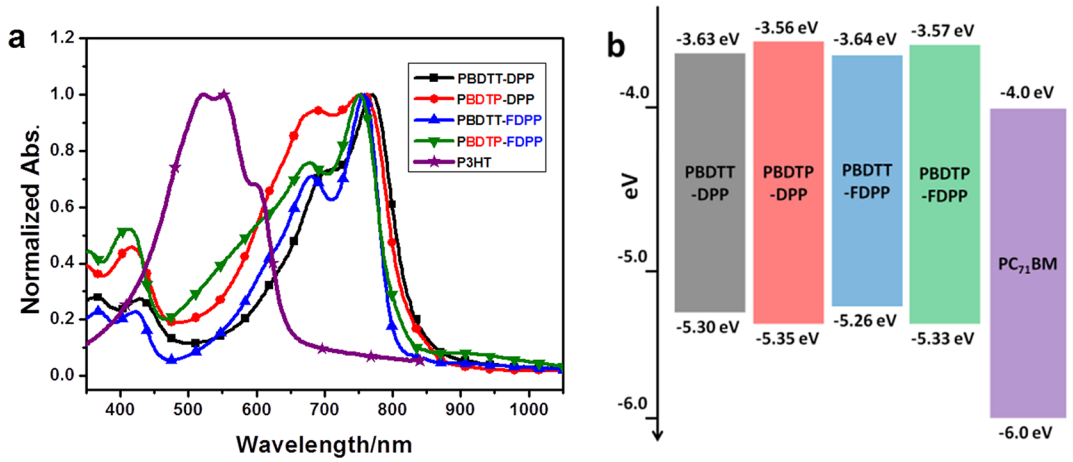

Figure 2. (a) UV−vis absorption spectra of the polymer films. (b) HOMO and LUMO energy levels of the polymers. Energy levels of $PC_{71}BM$ are listed for comparison.

dx.doi.org/10.1021/ja301460s | J. Am. Chem. Soc. XXXX, XXX, XXX−XXX

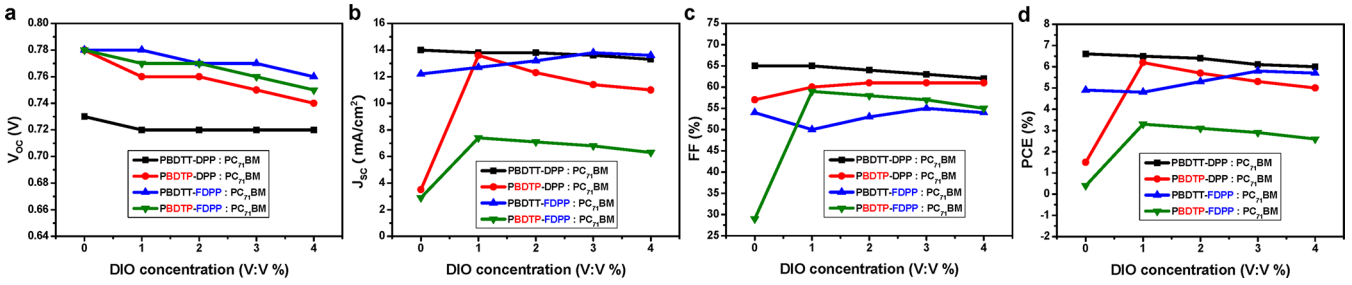

Figure 3. Solvent additive (DIO) concentration dependence of regular single layer solar cell performance of PBDTT-DPP, PBDTP-DPP, PBDTT-FDPP, and PBDTP-FDPP: (a) V_{OC}, (b) J_{SC}, (c) FF, and (d) PCE.

fabricated from the new polymers. For V_{OC} (Figure 3a), PBDTP-DPP, PBDTT-FDPP, and PBDTP-FDPP showed 0.05 V higher values than PBDTT-DPP at 0% DIO condition, indicating our design was successful in lowering the HOMO level to enhance the V_{OC} of the devices by introducing benzene and furan moieties into the polymers. As the DIO concentration increases, all of them show slightly lower V_{OC}. V_{OC}'s (0.7−0.8 V) for these polymers were notably higher than those for previously reported LBG materials due to their deeper HOMO levels (a detailed comparison correlating HOMO levels and V_{OC}'s can be found in the Supporting Information, Table S1). For J_{SC} (Figure 3b), without adding DIO, PBDTP-DPP and PBDTP-FDPP showed very low J_{SC}'s, probably due to the poor morphology of the blends; upon adding DIO, all of them except PBDTT-DPP showed enhanced J_{SC}. Devices made from PBDTP-DPP and PBDTT-FDPP can reach around 14 mA/cm^2 at 1% and 3% DIO, respectively. The low J_{SC} obtained for PBDTP-FDPP may be due to the morphology not being fully optimized through adding DIO. The fill factors of different materials (Figure 3c) showed different responses to DIO. As the DIO concentration increased, the FF of PBDTT-DPP decreased slightly (from 65% to 62%) and PBDTP-DPP increased slightly (from 57% to 60%); FF of PBDTT-FDPP decreased to 48% at 1% DIO and then went to a peak value of 55% at 3% DIO; the FF of PBDTP-FDPP increased dramatically from 28% to 59% upon adding 1% DIO and decreased slightly at higher DIO concentration. Thus, as shown in Figure 3d, the PCE of PBDTT-DPP showed its highest value of 6.6% at 0% DIO and decreased slightly at higher DIO concentrations; both PBDTP-DPP and PBDTP-FDPP showed their maximum values of 6.2% and 3.3% at 1% DIO, while PBDTT-FDPP showed the highest value of 5.8% at 3% DIO. It is interesting to note that the highest PCE of 6.6% for a single junction device was achieved without using DIO during the processing, which is a very unique property of this polymer. The characteristic properties of regular single layer BHJ solar cells are summarized in Table 2, and the J−V characteristics and EQEs for the best devices are shown in Figure 4. Among the four polymers, three of them gave PCEs around 6% under the optimized conditions. From EQE results (Figure 4b), broad response ranges covering 350−850 nm were obtained with average EQEs of 48% within this region for PBDTT-DPP, PBDTP-DPP, and PBDTT-FDPP. Besides the photovoltaic performance, the effects of adding DIO on the optical properties and the hole mobility of the polymers in the blend film have been investigated. As shown in Figure S5 (see the Supporting Information), because the UV−vis absorption spectra of the films only showed a very slight red-shift, and the SCLC mobility of the polymers was not increased dramatically after adding DIO as additive (Supporting Information, Table S2), the significant enhancement of the photovoltaic performance is most likely due to better film morphology.

Table 2. Characteristic Properties of Regular Single Layer BHJ Solar Cells

polymers	solvent	D:A	V_{OC} (V)	J_{SC} (mA/cm^2)	FF (%)	$PCE_{max}/_{ave}$ (%)
PBDTT-DPP	DCB	1:2	0.73	14.0	65	6.6/6.5
PBDTP-DPP	CF[a]	1:2	0.76	13.6	60	6.2/6.0
PBDTT-FDPP	DCB[b]	1:2	0.77	13.8	55	5.8/5.5
PBDTP-FDPP	DCB[c]	1:2	0.77	7.42	59	3.3/3.0

[a]1% DIO was added to the solution. [b]3% DIO was added to the solution. [c]1% DIO was added to the solution.

Morphology Studies. Polymer:$PC_{71}BM$ blend film morphology was investigated using atomic force microscopy (AFM). AFM phase images of films cast without DIO and with optimized DIO concentration are shown in Figure 5. For PBDTT-DPP (Figure 5a and b) and PBDTT-FDPP (Figure 5e and f), film morphology was almost identical, and the photovoltaic performance of the devices fabricated with and without DIO was similar. This is consistent with the measured J−V characteristics as shown in Figure 3. However, for PBDTP-DPP (Figure 5c and d) and PBDTP-FDPP (Figure 5g and h), dramatic changes in the film morphology were observed. Without DIO, high surface roughness and very weak phase separation were obtained for PBDTP-DPP:$PC_{71}BM$ (Figure 5c) and PBDTP-FDPP:$PC_{71}BM$ (Figure 5g) blend films. The nonoptimized morphology was probably due to fast drying of the solvent (CF) for PBDTP-DPP:$PC_{71}BM$ and extraordinarily good miscibility between polymers and $PC_{71}BM$. Nanoscale phase separation was achieved by adding 1% DIO as cosolvent for PBDTP-DPP:$PC_{71}BM$ (Figure 5d) and PBDTP-FDPP:$PC_{71}BM$ (Figure 5h) blends, respectively. Because of the more optimized morphology, both of the polymers showed significant enhancement of J_{SC} and FF, which lead to an increase in PCE from 1.5% to 6.2% for PBDTP-DPP and 0.4% to 3.3% for PBDTP-FDPP. Although DIO had a great effect on film morphology for PBDTP-FDPP-based devices, the maximum PCE was still not as high as other polymers. This can be attributed to the nonoptimum morphology of PBDTP-FDPP-based devices. As compared to Figure 5b, d, f, larger phase-separated features throughout the PBDTP-FDPP:$PC_{71}BM$ film were observed in Figure 5h.

Inverted Tandem Solar Cell Performance. Tandem polymer solar cells with inverted configuration[24,44] were

dx.doi.org/10.1021/ja301460s | J. Am. Chem. Soc. XXXX, XXX, XXX−XXX

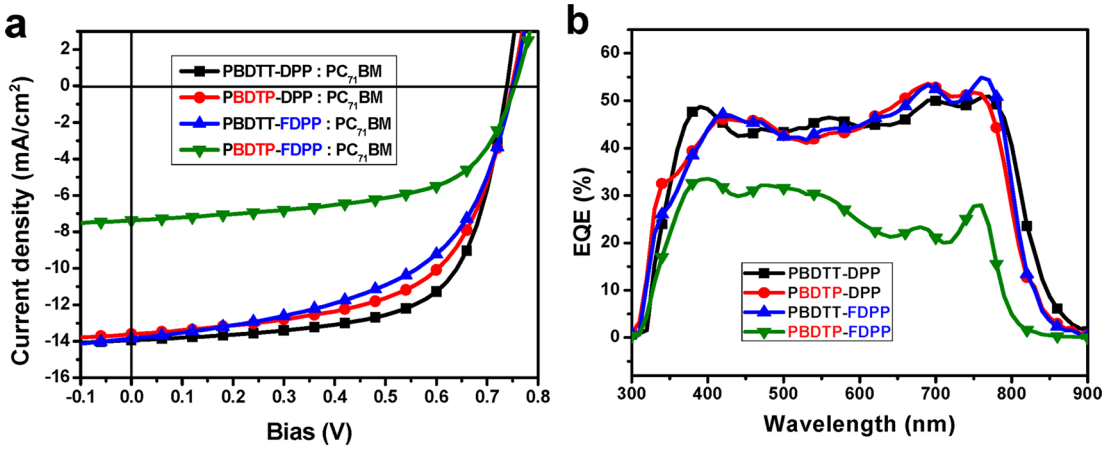

Figure 4. (a) Current–voltage characteristics of polymer/$PC_{71}BM$ solar cells under AM 1.5 condition (100 mW/cm^2). (b) EQEs of the corresponding devices.

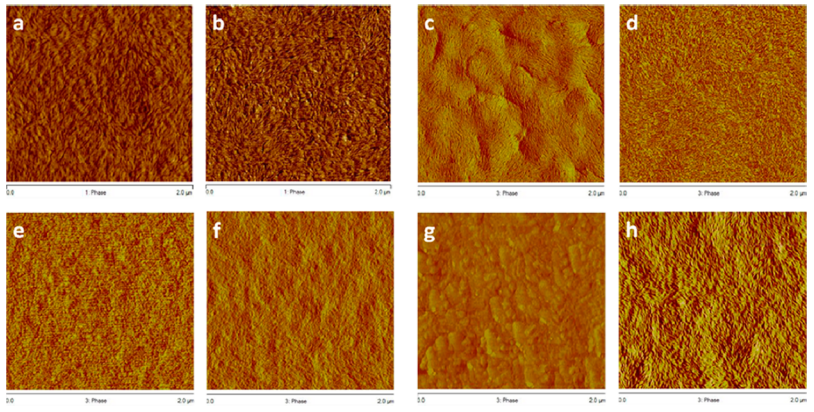

Figure 5. AFM phase images of polymer:$PC_{71}BM$ blend films: (a) PBDTT-DPP:$PC_{71}BM$ without DIO, (b) PBDTT-DPP:$PC_{71}BM$ with 2% DIO, (c) PBDTP-DPP:$PC_{71}BM$ without DIO, (d) PBDTP-DPP:$PC_{71}BM$ with 1% DIO, (e) PBDTT-FDPP:$PC_{71}BM$ without DIO, (f) PBDTT-FDPP:$PC_{71}BM$ with 3% DIO, (g) PBDTP-FDPP:$PC_{71}BM$ without DIO, and (h) PBDTP-FDPP:$PC_{71}BM$ with 1% DIO.

fabricated using the newly designed LBG polymers as the rear cell donor materials (PBDTP-FDPP was not tested in tandem devices due to the poor performance in single junction devices). The device structure is ITO/ZnO(30 nm)/P3HT:$IC_{60}BA$(150 nm)/PEDOT:PSS(30 nm)/ZnO (30 nm)/LBG polymer:$PC_{71}BM$ (100 nm)/MoO_3 (5 nm)/Ag as shown in Figure S6 (see the Supporting Information).[37] It is worthy of noting that the HOMO levels of around −5.3 eV for these LBG polymers not only help to increase V_{oc}, but also could help to improve charge injection at interfaces between MoO_3 and low bandgap polymers.[45] The J–V characteristics of the tandem cells and the performance parameters are shown in Figure 6. The best devices based on PBDTT-DPP, PBDTP-DPP, and PBDTT-FDPP showed PCEs as high as 8.8%, 8.5%, and 8.3%, respectively. All of the devices showed V_{OC} of ∼1.6 V, which is equal to the sum of the single front and rear cells; high J_{SC} of ∼8.5 mA/cm^2 and FF over 60% were achieved, leading to high PCEs for the tandem devices. As compared to PBDTT-DPP-, PBDTP-DPP- and PBDTT-FDPP-based devices showed slightly higher V_{OC} but lower FF, which are in accordance with the results of single junction devices. It should be noted that the difference in FF was not as big as single junction devices (65%, 60%, and 55% for single cells and 66%, 64%, and 61% for tandem cells) because the FF of a tandem device is determined by the two subcells. When the photocurrents from both cells are almost equal, the FF will

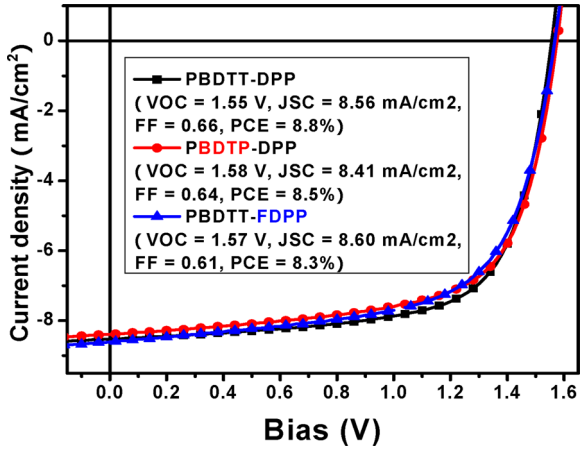

Figure 6. J–V characterstics of the tandem solar cells under AM1.5G illumination condition (100 mW/cm^2).

be the average of the two subcells.[43] Here, we have a P3HT-based front cell with J_{SC} around 9 mA/cm^2 and FF around 68% (see the Supporting Information, Figure S7), and thus the tandem devices would be expected to show FF around 66%, 64%, and 61% for PBDTT-DPP-, PBDTP-DPP-, and PBDTT-FDPP-based devices.

dx.doi.org/10.1021/ja301460s | J. Am. Chem. Soc. XXXX, XXX, XXX–XXX

The higher PCE achieved by using these three polymers as compared to other polymer systems[22−26] in tandem cells can be attributed to the simultaneous enhancement of V_{OC}, J_{SC}, and FF. Although pBBTDPP2-based tandem cells showed V_{OC} as high as 1.58 V, their J_{SC} and FF were much lower; whereas PCPDTBT-based tandem cells showed a high FF of 67% but a low V_{OC} of 1.2 V and J_{SC} of 7.6 mA/cm^2. Here, the V_{OC} of around 1.6 V and FF around 65% we obtained are among the highest values. More importantly, the high J_{SC} values of around 8.5 mA/cm^2 obtained here are more than 10% higher than the best reported data for tandem polymer solar cells (7.6 mA/cm^2) using other LBG polymers.[25,26] This can be attributed to the ability of PBDTT-DPP, PBDTP-DPP, and PBDTT-FDPP to utilize the low-energy portion (600−800 nm) of the solar irradiation very efficiently and enable balanced photocurrent from front and rear cells (external quantum efficiency of the tandem devices can be found in the Supporting Information, Figure S8, and the measurement details can be found in ref 37). It should be noted that during the peer review process of this Article, another high performance DPP derivative (PDPP5T) and its application in tandem PSCs with 7% PCE was reported by Janssen et al.[30] The drawback of the lower V_{OC} of the PDPP5T-based rear cell was compensated by using a PCDTBT-based front cell with higher V_{OC} than P3HT:ICBA. The overall PCE of the tandem was mainly limited by lower FF, probably due to the lower performance of the PCDTBT-based front cell or the ICL between the two subcells.

4. CONCLUSION

In summary, we have designed and synthesized a series of LBG polymers based on alternating modified BDT and DPP units for application in tandem PSCs. These new polymers showed low energy bandgap, deep HOMO energy level, and high hole mobility. Single junction devices achieved PCEs around 6% by morphology optimization. Tandem PSCs based on PBDTT-DPP, PBDTP-DPP, and PBDTT-FDPP showed high efficiencies reaching 9%. The significance of the newly developed LBG polymers is clearly demonstrated via their success in tandem devices, which showed simultaneously enhanced V_{OC}, J_{SC}, and FF over previously used LBG polymers such as PCPDTBT, PSBTBT, or pBBTDPP2 in tandem devices. We envision the work will pave the way for future materials design for tandem polymer solar cell to realize 15% efficiency.

■ ASSOCIATED CONTENT

Supporting Information

UV−visble absorption spectra, CV, SCLC results, tandem device structure, J−V characteristics of the P3HT:ICBA device, and EQEs of tandem devices. This material is available free of charge via the Internet at http://pubs.acs.org.

■ AUTHOR INFORMATION

Corresponding Author

yangy@ucla.edu

Notes

The authors declare no competing financial interest.

■ ACKNOWLEDGMENTS

This work was financially supported by the National Science Foundation (NSF), Air Force Office of Scientific Research (AFOSR), and Office of Naval Research (ONR). We thank Dr. Jun Yang, Mr. Xuanrong Guo, and Ms. Rene Green from UCLA for helpful discussion, material synthesis, and testing.

■ REFERENCES

(1) Cheng, Y. J.; Yang, S. H.; Hsu, C. S. *Chem. Rev.* **2009**, *109*, 5868.
(2) Li, G.; Zhu, R.; Yang, Y. *Nat. Photonics* **2012**, *6*, 153.
(3) Brabec, J.; Sariciftci, N. S.; Hummelen, J. C. *Adv. Funct. Mater.* **2011**, *11*, 15.
(4) Krebs, F. C. *Sol. Energy Mater. Sol. Cells* **2009**, *93*, 394.
(5) Li, G.; Shrotriya, V.; Huang, J. S.; Yao, Y.; Moriarty, T.; Emery, K.; Yang, Y. *Nat. Mater.* **2005**, *4*, 864.
(6) Peet, J.; Kim, J. Y.; Coates, N. E.; Ma, W. L.; Moses, D.; Heeger, A. J.; Bazan, G. C. *Nat. Mater.* **2007**, *6*, 497.
(7) Liang, Y. Y.; Feng, D. Q.; Wu, Y.; Tsai, S. T.; Li, G.; Ray, C.; Yu, L. P. *J. Am. Chem. Soc.* **2009**, *131*, 7792.
(8) Green, M. A.; Emery, K.; Hishikawa, Y.; Warta, W.; Dunlop, E. D. *Prog. Photovoltaics* **2011**, *19*, 565.
(9) Green, M. A.; Emery, K.; Hishikawa, Y.; Warta, W.; Dunlop, E. D. *Prog. Photovoltaics* **2012**, *20*, 12.
(10) Chen, H. Y.; Hou, J. H.; Zhang, S. Q.; Liang, Y. Y.; Yang, G. W.; Yang, Y.; Yu, L. P.; Wu, Y.; Li, G. *Nat. Photon.* **2009**, *3*, 649−653.
(11) Liang, Y. Y.; Xu, Z.; Xia, J.; Tsai, S. T.; Wu, Y.; Li, G.; Ray, C.; Yu, L. P. *Adv. Mater.* **2010**, *22*, E135−E138.
(12) He, Z. C.; Zhong, C. M.; Huang, X.; Wong, W. Y.; Wu, H. B.; Chen, L. W.; Su, S. J.; Cao, Y. *Adv. Mater.* **2011**, *23*, 4636.
(13) Würfel, W. *Physics of Solar Cells*; Wiley-VCH Verlag GmbH & Co. KgaA: Weinheim, 2005.
(14) King, R. R.; Law, D. C.; Edmondson, K. M.; Fetzer, C. M.; Kinsey, G. S.; Yoon, H.; Sherif, R. A.; Karam, N. H. *Appl. Phys. Lett.* **2007**, *90*, 183516.
(15) Wang, X. H.; Koleilat, G. I.; Tang, J.; Liu, H.; Kramer, I. J.; Debnath, R.; Brzozowski, L.; Barkhouse, D. A. R.; Levina, L.; Hoogland, S.; Sargent, E. H. *Nat. Photonics* **2011**, *5*, 480.
(16) Riede, M.; Uhrich, C.; Widmer, J.; Timmreck, R.; Wynands, D.; Schwartz, G.; Gnehr, W.-M.; Hildebrandt, D.; Weiss, A.; Hwang, J.; Sundarraj, S.; Erk, P.; Pfeiffer, M.; Leo, K. *Adv. Funct. Mater.* **2011**, *21*, 3019.
(17) Xue, J.; Uchida, S.; Rand, B. P.; Forrest, S. R. *Appl. Phys. Lett.* **2004**, *85*, 5757.
(18) Shockley, W.; Queisser, H. J. *J. Appl. Phys.* **1961**, *32*, 510.
(19) Scharber, M. C.; Muhlbacher, D.; Koppe, M.; Denk, P.; Waldauf, C.; Heeger, A. J.; Brabec, C. J. *Adv. Mater.* **2006**, *18*, 789.
(20) Dennler, G.; Scharber, M. C.; Ameri, T.; Denk, P.; Forberich, K.; Waldauf, C.; Brabec, C. J. *Adv. Mater.* **2008**, *20*, 579.
(21) Hadipour, A.; de Boer, B.; Wildeman, J.; Kooistra, F. B.; Hummelen, J. C.; Turbiez, M. G. R.; Wienk, M. M.; Janssen, R. A. J.; Blom, P. W. M. *Adv. Funct. Mater.* **2006**, *16*, 1897.
(22) Sista, S.; Park, M. H.; Hong, Z. R.; Wu, Y.; Hou, J. H.; Kwan, W. L.; Li, G.; Yang, Y. *Adv. Mater.* **2010**, *22*, 380.
(23) Gilot, J.; Wienk, M. M.; Janssen, R. A. J. *Adv. Mater.* **2010**, *22*, E67.
(24) Chou, C. H.; Kwan, W. L.; Hong, Z. R.; Chen, L. M.; Yang, Y. *Adv. Mater.* **2011**, *23*, 1282.
(25) Kim, J. Y.; Lee, K.; Coates, N. E.; Moses, D.; Nguyen, T. Q.; Dante, M.; Heeger, A. J. *Science* **2007**, *317*, 222.
(26) Yang, J.; Zhu, R.; Hong, Z.; Kumar, A.; Yang, Y. *Adv. Mater.* **2011**, *23*, 3465.
(27) Tung, V. C.; Kim, J.; Cote, L. J.; Huang, J. X. *J. Am. Chem. Soc.* **2011**, *133*, 9262.
(28) Tung, V. C.; Kim, J.; Cote, L. J.; Huang, J. X. *Adv. Energy Mater.* **2012**, *2*, 299.
(29) Kouijzer, S.; Esiner, S.; Frijters, C. H.; Turbiez, M.; Wienk, M. M.; Janssen, R. A. J. *Adv. Energy Mater.* **2012**, DOI: 10.1002/aenm.201100773.
(30) Gevaerts, V. S.; Furlan, A.; Wienk, M. M.; Turbiez, M.; Janssen, R. A. J. *Adv. Mater.* **2012**, *24*, 2130.
(31) Hou, J. H.; Chen, H. Y.; Zhang, S. Q.; Li, G.; Yang, Y. *J. Am. Chem. Soc.* **2008**, *130*, 16144.

(32) Tieke, B.; Rabindranath, A. R.; Zhang, K.; Zhu, Y. *Beilstein J. Org. Chem.* **2010**, *6*, 830.
(33) Bijleveld, J. C.; Zoombelt, A.; Mathijssen, S. G. J.; Wienk, M. M.; Turbiez, M.; de Leeuw, D. M.; Janssen, R. A. J. *J. Am. Chem. Soc.* **2009**, *131*, 16616.
(34) Bijleveld, J. C.; Gevaerts, V. S.; Di Nuzzo, D.; Turbiez, M.; Mathijssen, S. G. J.; de Leeuw, D. M.; Wienk, M. M.; Janssen, R. A. J. *Adv. Mater.* **2010**, *22*, E242.
(35) Woo, C. H.; Beaujuge, P. M.; Holcombe, T. W.; Lee, O. P.; Fréchet, J. M. J. *J. Am. Chem. Soc.* **2010**, *132*, 15547.
(36) Huo, L.; Hou, J.; Chen, H.-Y.; Zhang, S.; Jiang, Y.; Chen, T.; Yang, Y. *Macromolecules* **2009**, *42*, 6564.
(37) Dou, L. T.; You, J. B.; Yang, J.; Chen, C.-C.; He, Y. J.; Murase, S.; Moriarty, T.; Emery, K.; Li, G.; Yang, Y. *Nat. Photonics* **2012**, *6*, 180.
(38) He, Y. J.; Chen, H.-Y.; Hou, J. H.; Li, Y. F. *J. Am. Chem. Soc.* **2010**, *132*, 1377.
(39) Beek, W. J. E.; Wienk, M. M.; Janssen, R. A. J. *Adv. Mater.* **2004**, *16*, 1009.
(40) Goh, C.; Kline, R. J.; McGehee, M. D.; Kadnikova, E. N.; Frechet, J. M. J. *Appl. Phys. Lett.* **2005**, *86*, 122110.
(41) Huo, L. J.; Hou, J. H.; Zhang, S. Q.; Chen, H.-Y.; Yang, Y. *Angew. Chem., Int. Ed.* **2011**, *50*, 1.
(42) Piliego, C.; Holcombe, T. W.; Douglas, J. D.; Woo, C. H.; Beaujuge, P. M.; Fréchet, J. M. J. *J. Am. Chem. Soc.* **2010**, *132*, 7595.
(43) Burdick, J.; Glatfelter, T. *Sol. Cells* **1986**, *18*, 301.
(44) Li, G.; Chu, C.-W.; Shrotriya, V.; Huang, J.; Yang, Y. *Appl. Phys. Lett.* **2006**, *88*, 253503.
(45) Wang, X.; Koleilat, G. I.; Fischer, A.; Tang, J.; Debnath, R.; Levina, L.; Sargent, E. H. *ACS Appl. Mater. Interfaces* **2011**, *3*, 3792.